Journal of Statistical Physics, Vol. 64, Nos. 5/6, 1991

Fluctuating Hydrodynamics and Principal Oscillation Pattern Analysis

Alejandro García[1] **and Cécile Penland**[2]

Principal oscillation pattern (POP) analysis was recently introduced into climatology to analyze multivariate time series $x_i(t)$ produced by systems whose dynamics are described by a linear Markov process $\dot{\mathbf{x}} = \mathbf{B}\mathbf{x} + \xi$. The matrix $\mathbf{B}$ gives the deterministic feedback and ξ is a white noise vector with covariances $\langle \xi_i(t)\, \xi_j(t') \rangle = Q_{ij}\delta(t - t')$. The POP method is applied to data from a direct simulation Monte Carlo program. The system is a dilute gas with 50,000 particles in a Rayleigh–Bénard configuration. The POP analysis correctly reproduces the linearized Navier–Stokes equations (in the matrix $\mathbf{B}$) and the stochastic fluxes (in the matrix $\mathbf{Q}$) as given by Landau–Lifschitz fluctuating hydrodynamics. Using this method, we find the Landau–Lifschitz theory to be valid both in equilibrium and near the critical point of Rayleigh–Bénard convection.

KEY WORDS: Fluctuating hydrodynamics; Rayleigh–Bénard convection; Langevin equation; principal oscillation pattern analysis.

1. INTRODUCTION

Rayleigh–Bénard convection is a paradigm instability; at a critical Rayleigh number there is a bifurcation between states of purely conductive heat flow and buoyancy-driven convection.[1] The nature of the hydrodynamic fluctuations near this transition point has been studied theoretically by a variety of methods.[2] The Santa Barbara group has performed several careful experiments and has measured the variation in the heat flux near the onset of convection.[3] Quantitative comparison between fluctuating hydrodynamics calculations and laboratory experiments reveals significant,

[1] Department of Physics, San Jose State University, San Jose, California 95192-0106.
[2] Cooperative Institute for Research in the Environmental Sciences, University of Colorado, Boulder, Colorado 80309-2016.

0022-4715/91/0900-1121$06.50/0

unaccountable discrepancies.[4] In this context, new methods for studying fluctuation phenomena are welcome. In this paper, principal oscillation pattern (POP) analysis, a statistical technique developed in climatology,[5] is used to analyze data from a particle simulation of a dilute gas near the onset of convection. The POP method may be seen as an extension of the traditional use of correlation functions; it has the advantage that very little is assumed about the form of the linearized equations.

2. FLUCTUATING HYDRODYNAMICS

Landau and Lifschitz proposed that thermal fluctuations at the molecular level could be modeled by adding a random component to the stress tensor and the heat flux in the Navier–Stokes equations.[6] In the case where the density ρ_0, the velocity $\mathbf{V}_0 = 0$, and the temperature T_0 are the deterministic, steady-state solutions, and where $\delta\rho$, $\delta\mathbf{V}$, and δT are the fluctuations around the steady-state solutions, the linearized hydrodynamic equations are

$$\frac{\partial \delta\rho}{\partial t} = -\rho_0 \nabla \cdot \delta\mathbf{V} \tag{1a}$$

$$\rho_0 \frac{\partial \delta\mathbf{V}}{\partial t} = -\nabla \delta P - \delta\rho\, g\mathbf{j} - \mu\nabla \times [\nabla \times \delta\mathbf{V}] + \nabla[(\lambda + \tfrac{4}{3}\mu)\nabla \cdot \delta\mathbf{V}] - \nabla \cdot \mathbf{S} \tag{1b}$$

$$\rho_0 c_v \frac{\partial \delta T}{\partial t} = -P_0 \nabla \cdot \delta\mathbf{V} + \kappa\nabla^2 \delta T - \nabla \cdot \mathbf{q} \tag{1c}$$

where P is the pressure, g is gravitational acceleration, and the transport coefficients are: μ, shear viscosity; λ, bulk viscosity ($=0$ for a dilute gas); and κ, thermal conductivity. The unit vector in the y direction is $\mathbf{j}$.

The white noise parts of stress tensor $\mathbf{S}$ and heat flux $\mathbf{q}$ have zero mean and variance,

$$\langle S_{ij}(\mathbf{r}, t)\, S_{kl}(\mathbf{r}', t')\rangle = 2k_B \mu T(\delta_{ik}\delta_{jl} + \delta_{il}\delta_{jk} - \tfrac{2}{3}\delta_{ij}\delta_{kl}) \times \delta(\mathbf{r} - \mathbf{r}')\, \delta(t - t') \tag{2a}$$

$$\langle q_i(\mathbf{r}, t)\, q_j(\mathbf{r}', t')\rangle = 2k_B \kappa T^2 \delta_{ij} \delta(\mathbf{r} - \mathbf{r}')\, \delta(t - t') \tag{2b}$$

where δ_{ij} is the Kronecker delta, $\delta(x)$ is the Dirac delta function, and k_B is Boltzmann's constant.

The Navier–Stokes equations may be discretized on an $N \times M$ grid; let (i, j) be indices designating the location $x = i\Delta$, $y = j\Delta$. The spatial

derivatives are replaced by their discretized forms; for example, the Laplacian terms are transformed as

$$\nabla^2 f = \frac{1}{\Delta^2}\left[f(i+1, j) + f(i-1, j) + f(i, j+1) + f(i, j-1) - 4f(i, j)\right] \quad (3)$$

We can then express the fluctuating Navier–Stokes equations in the form

$$\frac{d}{dt}\mathbf{x} = \mathbf{B}\mathbf{x} + \xi \quad (4)$$

by using the construction

$$\mathbf{x}^T = (\delta\rho(1, 1), \delta V_x(1, 1), \delta V_y(1, 1), \delta V_z(1, 1), \delta T(1, 1), \ldots,$$
$$\delta\rho(N, M), \delta V_x(N, M), \delta V_y(N, M), \delta V_z(N, M), \delta T(N, M)) \quad (5)$$

The variance of the white noise is $\langle \xi_i(t)\, \xi_j(t')\rangle = Q_{ij}\delta(t-t')$.

The matrix **B** contains the linearized Navier–Stokes equations. For example, in a dilute gas, the density affects the change in the y component of velocity through the pressure term in Eq. (1b) as

$$\rho_0 \frac{\partial \delta V_y}{\partial t} = -RT_0 \frac{\partial \delta\rho}{\partial y} + \cdots \quad (6)$$

since the pressure is $P = \rho RT$. The corresponding term in the matrix **B** is

$$B_{ij;i'j'}^{v_y\rho} = -\frac{RT_0}{2\rho_0\Delta}\left(\delta_{j+1,j'} - \delta_{j-1,j'}\right)\delta_{i,i'} \quad (7)$$

The y component of velocity is coupled to itself through the viscous term in the velocity equation (1b):

$$\rho_0 \frac{\partial \delta V_y}{\partial t} = \mu\left(\frac{\partial^2 \delta V_y}{\partial x^2} + \frac{4}{3}\frac{\partial^2 \delta V_y}{\partial y^2}\right) + \cdots \quad (8)$$

The corresponding term in the matrix **B** is

$$B_{ij;i'j'}^{v_y v_y} = \frac{\mu}{\rho_0\Delta^2}\left\{\left(\delta_{i+1,i'} + \delta_{i-1,i'} - 2\delta_{i,i'}\right)\delta_{j,j'} + \frac{4}{3}\left(\delta_{j+1,j'} + \delta_{j-1,j'} - 2\delta_{j,j'}\right)\delta_{i,i'}\right\} \quad (9)$$

In Section 5, we see that the POP analysis can reconstruct these **B** coefficients from the time series $\mathbf{x}(t)$.

3. PRINCIPAL OSCILLATION PATTERN (POP) ANALYSIS

For the linear Markov process, $\dot{\mathbf{x}} = \mathbf{B}\mathbf{x} + \xi$, the principal oscillation patterns (POPs) are the eigenfunctions of the deterministic feedback matrix $\mathbf{B}$.[5,7] In other words, the POPs are the empirically computed eigenmodes of the system. We identify the Green function

$$\mathbf{G}(\tau) = \exp(\mathbf{B}\tau) = \langle \mathbf{x}(t+\tau)\,\mathbf{x}^T(t)\rangle \langle \mathbf{x}(t)\,\mathbf{x}^T(t)\rangle^{-1} \tag{10}$$

The POP analysis obtains an estimate for $\mathbf{B}$ as follows: Given a time series $\mathbf{x}(t)$, one calculates the matrices $\langle \mathbf{x}(t)\,\mathbf{x}^T(t)\rangle$ and $\langle \mathbf{x}(t+\tau)\,\mathbf{x}^T(t)\rangle$ and forms $\mathbf{G}$. The eigenvalues $g_\alpha \equiv \exp(\beta_\alpha \tau)$ and eigenvectors $\mathbf{u}_\alpha$ of $\mathbf{G}$ are computed as well as the eigenvectors $\mathbf{v}_\alpha$ of $\mathbf{G}^T$. One obtains the eigenvalues β_α of $\mathbf{B}$ from the eigenvalues g_α of $\mathbf{G}$ and forms the deterministic feedback matrix as

$$\mathbf{B} = \sum_\alpha \mathbf{u}_\alpha \beta_\alpha \mathbf{v}_\alpha^T \tag{11}$$

After finding $\mathbf{B}$, the equal-time covariance of the noise $\langle \xi_i \xi_j \rangle \equiv Q_{ij}$ is calculated as

$$\mathbf{Q} = -(\mathbf{B}\langle \mathbf{x}(t)\,\mathbf{x}^T(t)\rangle + \langle \mathbf{x}(t)\,\mathbf{x}^T(t)\rangle\,\mathbf{B}^T) \tag{12}$$

Note that $\mathbf{B}$ and $\mathbf{Q}$ are obtained solely from the time series data $\mathbf{x}(t)$. If the system is well described by a linear Markov process, then our estimate of $\mathbf{B}$ and $\mathbf{Q}$ will be independent of the choice of τ.[3] On the other hand, if nonlinear effects are important, then $\mathbf{B}$ and $\mathbf{Q}$ will vary significantly with τ.

4. DILUTE GAS SIMULATION

We use the direct simulation Monte Carlo (DSMC) method[8] to simulate a dilute gas of 50,000 hard spheres. The method has been used successfully to study fluctuations in simple nonequilibrium systems.[9] In this paper, the geometry is a square container with periodic boundary conditions in the z direction; the length of a side L equals 50 mean free paths. The top and bottom walls ($y = 0, L$) are slip, thermal walls, while the sides ($x = 0, L$) are slip, insulated walls. Typical run length is about 10^8 collisions (10^3–10^4 timesteps). The container is divided into 100 boxes of equal size and at each timestep the density, velocity, and temperature are measured in each box. These data are used to construct the vector $\mathbf{x}(t)$ to which the POP analysis is applied. All runs were performed on a Sun 4/260 workstation.

[3] Some values of τ will give greater accuracy. A POP with eigenvalue β is most accurately obtained when $\tau = -1/\mathrm{Re}\,\beta$.

5. POP ANALYSIS: NONCONVECTING CASES

The first case we consider is an equilibrium system. The POPs for the stream function agree with the known equilibrium eigenmodes for slip boundaries, $\phi_{mn} = \sin(m\pi/L)\sin(n\pi/L)$, $m, n = 1, 2, \ldots$. A contour map of the fourth POP ($m = n = 2$) is shown in Fig. 1. Ordering the POPs in decreasing e-folding time $\tau_\alpha = 1/\mathrm{Re}(\beta_\alpha)$, we find that the e-folding time varies as $\tau_\alpha \propto 1/(m^2 + n^2)$. In the deterministic feedback matrix **B**, the effect of density on the y component of the velocity is given by Eq. (7). For a location near the center of the system, the POP analysis reproduced this form, as shown in Fig. 2. Similarly, the effect of the y component of the velocity on itself is given by Eq. (9). For a location near the center of the system, the POP analysis reproduced this form, as shown in Fig. 3. These examples show that the POP method can reconstruct the linearized Navier–Stokes equations from the time series.

For the noise covariance in the x component of the velocity, fluctuating hydrodynamics predicts

$$Q^{v_x}_{ij;i'j'} = -\frac{2k_B\mu T_0}{\Delta^2\rho_0^2}\left\{\frac{4}{3}(\delta_{i+1,i'} + \delta_{i-1,i'} - 2\delta_{i,i'})\,\delta_{j,j'} + (\delta_{j+1,j} + \delta_{j-1,j} - 2\delta_{j,j'})\,\delta_{i,i'}\right\} \tag{13}$$

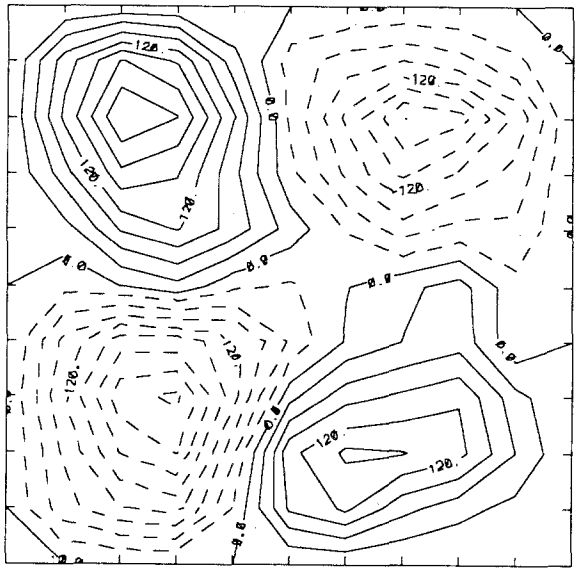

Fig. 1. Contour plot of the stream function for the fourth principal oscillation pattern obtained from the time series. Solid lines are positive contours; dashed lines are negative contours. Compare with $\phi_{22} = \sin(2\pi x/L)\sin(2\pi y/L)$.

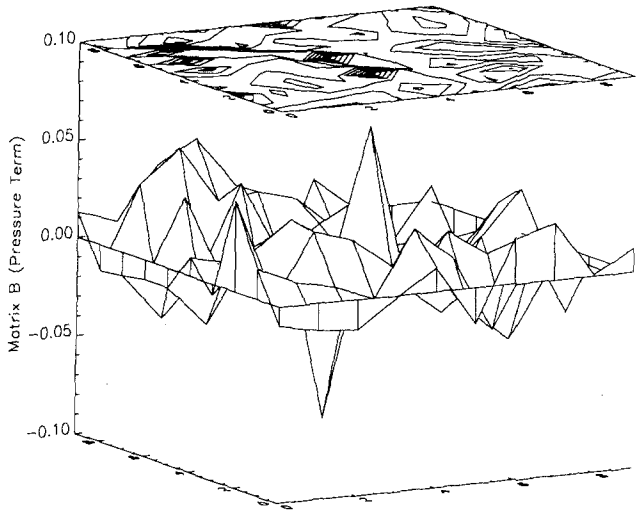

Fig. 2. Landscape and contour plot of $B^{v_y\rho}_{ij;i'j'}$ [see Eq. (7)] for $i=4$, $j=4$. The system is at equilibrium. This is the pressure term in the δV_y equation. We expect a peak at $i'=4$, $j'=3$ and an equal trough at $i'=4$, $j'=5$.

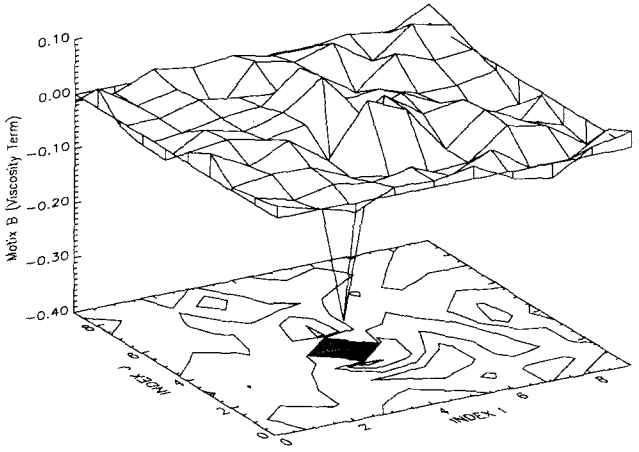

Fig. 3. Landscape and contour plot of $B^{v_y v_y}_{ij;i'j'}$ [see Eq. (9)] for $i=4$, $j=4$. The system is at equilibrium. This is the viscosity term in the δV_y equation. We expect a trough at $i'=4$, $j'=4$ and a peak at each of the four nearest-neighbor points.

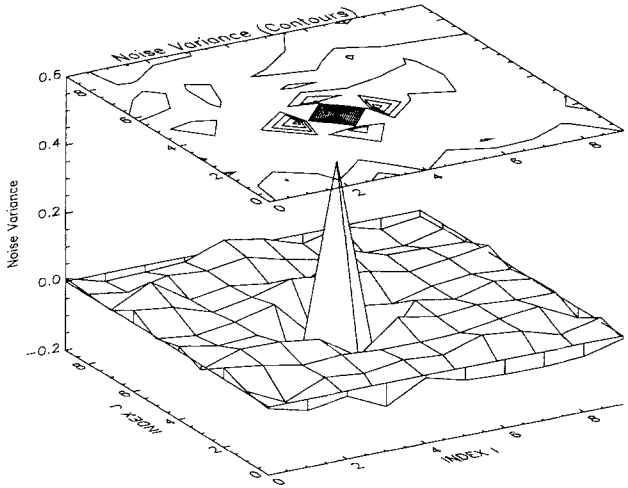

Fig. 4. Landscape and contour plot of $Q^{v_x}_{ij;i'j'}$ [see Eq. (13)] for $i=4$, $j=4$. The system is at equilibrium. We expect a peak at $i'=4$, $j'=4$ and a trough at each of the four nearest-neighbor points.

This function has a strong peak at $i=i'$, $j=j'$ and smaller troughs at the four nearest-neighbor points. For a location near the center of the system, the results from the POP analysis are shown in Fig. 4. Good results are also obtained for the noise variances in the y component of velocity and temperature.

Using the POP analysis, we compute the temperature dependence of the amplitude of the noise. We simulated a system without gravity in the

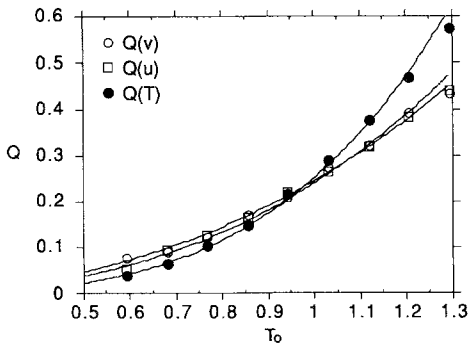

Fig. 5. Noise variance as a function of temperature in a system with a linear temperature gradient (i.e., conduction state). The open squares and circles are Q^{v_x} and Q^{v_y}, respectively. The solid circles are Q^T. Solid lines are the least-square power law fit to the data. Compare with Eqs. (14)–(16).

conduction state (linear temperature gradient). From fluctuating hydrodynamics, the noise variance for the velocity is

$$Q^{v_x} \quad \text{or} \quad Q^{v_y} \propto \frac{\mu(T_0)\, T_0}{\rho_0^2} \propto T_0^{5/2} \tag{14}$$

since $\mu(T_0) \propto \sqrt{T_0}\,\rho_0$ and $\rho_0 \propto 1/T_0$ (the pressure is constant in the system). The noise variance for the temperature is

$$Q^T \propto \frac{\kappa(T_0)\, T_0^2}{\rho_0^2} \propto T_0^{7/2} \tag{15}$$

since $\kappa(T_0) \propto \sqrt{T_0}\,\rho_0$. The POP analysis for a system in the conduction state gives

$$Q^{v_x} \propto T_0^{2.65}, \qquad Q^{v_y} \propto T_0^{2.37}, \qquad Q^T \propto T_0^{3.47} \tag{16}$$

These results are presented in Fig. 5. These last two figures show that the analysis can reconstruct the noise variances from the time series.

6. POP ANALYSIS: RAYLEIGH–BÉNARD CONVECTION

For a dilute gas, the density profile in the conducting state goes as $\rho_0 \propto T_0^a$, where $a = mgL/k_B\,\Delta T - 1$, the mass of a particle is m, and ΔT is the vertical temperature gradient. By taking the value of the gravitational field as $g = k_B\,\Delta T/mL$, the density is constant throughout the system. For a dilute gas, the Rayleigh number may be written as

$$R = (256/125\pi)(\Delta T/T_0)^2\,(L/\lambda)^2 \tag{17}$$

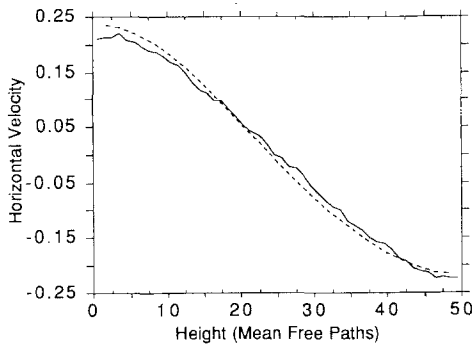

Fig. 6. Horizontal (x) velocity versus height (y) in a vertical slice through the center of the system. The convection is fully developed, the Rayleigh number is well above critical ($R \approx 1.7R_c$). The solid line is the average velocity measured in the DSMC simulation. The dashed line is the numerical solution of the deterministic Navier–Stokes equations.

where λ is the mean free path in the gas. In our system, since the walls were slip-slip and the aspect ratio was unity, the critical Rayleigh number was $R_c \approx 780$.[1]

We first simulated a system well above the critical Rayleigh number ($R = 1357 \approx 1.7 R_c$). Comparing the flow field obtained in the DSMC simulation with the numerical solution of the deterministic Navier–Stokes equations, we find excellent quantitative agreement (see Figs. 6 and 7).

The POP analysis was performed on the data from the particle simulation for a system near the critical Rayleigh number. The first POP is the mode which becomes unstable; its e-folding time increases dramatically (factor of 5), indicating critical slowing down. The e-folding time of all the other POPs remained close to their equilibrium values.

The spatial correlation of the noise is found to be very similar to its equilibrium form (see Fig. 8 and compare with Fig. 4). From fluctuating hydrodynamics, the noise variances are given by Eqs. (14) and (15). However, since the gravitational field maintains the density ρ_0 constant in the Rayleigh–Bénard system we have

$$Q^{v_x} \quad \text{or} \quad Q^{v_y} \propto T_0^{3/2} \qquad \text{and} \qquad Q^T \propto T_0^{5/2} \tag{18}$$

Using the data from the DSMC simulation for a system near the critical point, the POP analysis gives

$$Q^{v_x} \propto T_0^{1.19}, \qquad Q^{v_y} \propto T_0^{1.35}, \qquad Q^T \propto T_0^{2.35} \tag{19}$$

These results are illustrated in Fig. 9. These last two figures show that the noise terms in the Landau–Lifshitz fluctuating hydrodynamics retain their equilibrium form near the critical Rayleigh number.

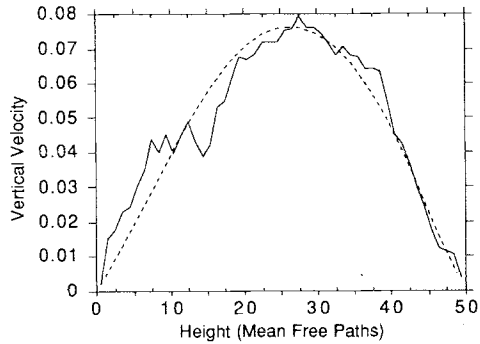

Fig. 7. Vertical (y) velocity versus height (y) in a vertical slice through the center of the system. See Fig. 6 caption for details.

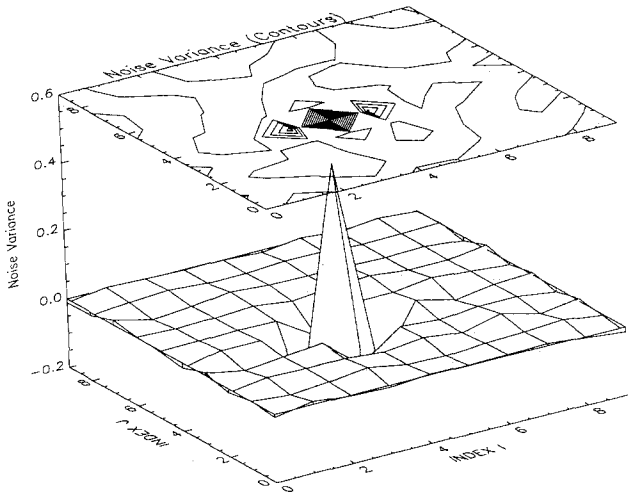

Fig. 8. Landscape and contour plot of $Q^{v_x}_{ij;i'j'}$ [see Eq. (13)] for $i=4$, $j=4$. The Rayleigh number in the system is near the critical value. Compare with Fig. 4.

The results presented here for the system near the critical Rayleigh number are still preliminary. For a number of reasons (e.g., temperature "jump" at the walls) it is difficult to measure precisely the distance from criticality. Ideally, we would like to ramp the temperature profile slowly through the critical point as is done in the laboratory experiments.[3] We hope to do some runs of this type in the near future.

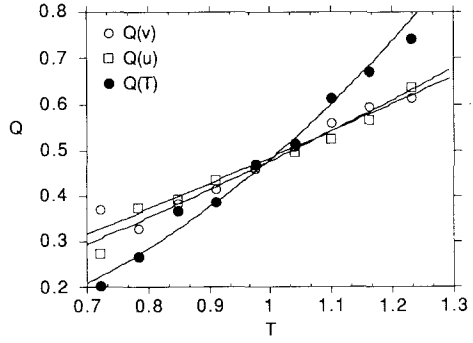

Fig. 9. Noise variance as a function of temperature in a system near the critical Rayleigh number. See Fig. 5 caption for details. Compare these results with the similar graph for the conduction state (Fig. 5); see also Eqs. (18) and (19).

7. CONCLUSION AND REMARKS

In this paper, we apply the principal oscillation pattern analysis to data from a particle simulation. The method does a reasonably good job of reconstructing the fluctuating hydrodynamics equations including the noise terms. While the POP method offers several advantages over more traditional methods, its main disadvantage is that longer time series are needed to accurately reconstruct **B** and **Q**. In the work presented here, the matrices **B** and **Q** are each 500×500 in size (five hydrodynamic variables; 100 spatial locations). The number of available data points in a typical run was 5×10^6 or about 10 data points per unknown coefficient. In a model examined in ref. 7 it is found that **B** and **Q** may be accurately reconstructed with as few as 10 data points per coefficient, depending on the eigenvalues of **B**.

In computer simulations, obtaining enough data is only a question of available resources; recall that all the work presented here was done on a workstation. While in some laboratory experiments it may be difficult to obtain enough data to use the POP method, we anticipate that modern computer-aided data acquisition will ameliorate this problem. For example, the POP analysis may be applied to the digitized video camera images from the electroconvection experiments described by Rehberg *et al.* in this proceedings.

ACKNOWLEDGMENTS

The authors wish to thank M. Blackman and the Climate Research Division of CIRES for computational support. We also thank M. Malek Mansour for the use of his Navier–Stokes solver and M. Ghil for useful discussions.

REFERENCES

1. S. Chandrasekhar, *Hydrodynamic and Hydromagnetic Stability* (Dover Press, New York, 1981).
2. V. M. Zaitsev and M. I. Shliomis, *Sov. Phys. JETP* **32**:866 (1971); H. N. W. Lekkerkerker and J. P. Boon, *Phys. Rev. A* **10**:1355 (1974); T. R. Kirkpatrick and E. G. D. Cohen, *J. Stat. Phys.* **33**:639 (1983); R. Schmitz and E. G. D. Cohen, *J. Stat. Phys.* **38**:285 (1985).
3. G. Ahlers, M. C. Cross, P. C. Hohenberg, and S. Safran, *J. Fluid Mech.* **110**:297 (1981); R. P. Behringer and G. Ahlers, *J. Fluid Mech.* **125**:219 (1982); C. W. Meyer, G. Ahlers, and D. S. Cannell, *Phys. Rev. Lett.* **59**:1577 (1987); G. Ahlers, C. Meyer, and D. Cannell, *J. Stat. Phys.* **54**:1121 (1989).
4. H. Van Beijeren and E. G. D. Cohen, *Phys. Rev. Lett.* **60**:1208 (1988); *J. Stat. Phys.* **53**:77 (1988).

5. K. Hasselmann, *Tellus* **28**:473 (1976); *J. Geophys. Res.* **93**:11, 105 (1988).
6. L. D. Landau and E. M. Lifshitz, *Fluid Mechanics* (Pergamon Press, Oxford, 1959).
7. C. Penland, *Monthly Weather Rev.* **117**:2165 (1989).
8. G. A. Bird, *Molecular Gas Dynamics* (Clarendon Press, Oxford, 1976).
9. A. Garcia, *Phys. Rev. A* **34**:1454 (1986); M. Malek Mansour, A. Garcia, G. Lie, and E. Clementi, *Phys. Rev. Lett.* **58**::874 (1987); A. Garcia, M. Malek Mansour, G. Lie, and E. Clementi, *J. Stat. Phys.* **47**:209 (1987).